J Mater Sci (2007) 42:7171–7175
DOI 10.1007/s10853-007-1577-y

Gas permeability behavior of mullite-bonded porous silicon carbide ceramics

Shuqiang Ding · Yu-Ping Zeng · Dongliang Jiang

Received: 9 January 2007 / Accepted: 31 January 2007 / Published online: 10 May 2007

Abstract An apparatus was developed to evaluate the gas permeability behavior of mullite ($3Al_2O_3{\cdot}2SiO_2$)-bonded porous silicon carbide (SiC) ceramics at room temperature. The permeability was calculated according to Forchheimer's equation for the compressible gas. It was found that the sintering temperature and graphite (pore former) addition during the fabrication of the porous ceramics affect the permeability extremely by varying the texture of porous ceramics such as the open porosity, pore size distribution and tortuosity of pore channels. The increased sintering temperature results in a decreased Darcian (viscous) permeability but an increased non-Darcian (inertial) permeability. However, more graphite additions lead to the larger Darcian and non-Darcian permeability.

Introduction

Porous silicon carbide (SiC) ceramics have been considered as one of the most favorite candidates for hot gas cleanup, melt metal filtration, catalytic substrate and thermal insulation, owing to their low bulk density, high permeability, high temperature stability, corrosion resistance and excellent catalytic activity [1–4]. Various processes, such as the particle stacking [5], pore former [6], template replication [7] and bubble generation [8], were developed to fabricate porous SiC ceramics. At the same time, the bulk density, open porosity, pore size distribution, strength, coefficient of thermal expansion, thermal shock resistance, high temperature-oxidation resistance and acid/alkaline endurance of porous SiC ceramics were also studied in detailed [9–11]. In practical applications, the permeability of porous media need be quantified to investigate the efficiency of the hot gas filtration in the porous catalytic substrate, coal-gasification-generation process and diesel exhaust system. However, very limited information about the permeability of porous ceramics exists in the literature [12–16]. Particularly, there have been even less attention to the gas permeability behavior of porous SiC ceramics with the micrometeric pore size [17].

In the present work, the gas permeability behavior of mullite ($3Al_2O_3{\cdot}2SiO_2$)-bonded porous SiC ceramics with the pore size of 0.1–20 μm and the open porosity of 25–62% was evaluated by a homemade permeability apparatus. Forchheimer's equation for the compressible gas was used to calculate the permeability. Effects of the sintering temperatures and graphite (pore former) additions during the fabrication on the permeability were investigated.

Description of permeability

For laminary viscous flow through the porous material, Darcy's law, which establishes a linear dependence between the pressure gradient and the fluid velocity through the porous medium, is expressed for the incompressible fluid as [18–20]

$$\frac{P_i - P_o}{L} = \frac{\eta}{K_1} V_s, \tag{1}$$

where P_i is the fluid pressure at the entrance (Pa); P_o is the fluid pressure at the sample exit (Pa); L is the sample thickness (m); η is the viscosity of the fluid (Pa·s); K_1 is the

S. Ding (✉) · Y.-P. Zeng · D. Jiang
Shanghai Institute of Ceramics, Chinese Academy of Sciences, 1295 Dingxi Road, Shanghai 200050, China
e-mail: sqding@mail.sic.ac.cn

Darcian or viscous permeability (m^2); V_s is the fluid velocity (m/s), given by the volumetric flow rate divided by the sample cross-sectional area. Darcian permeability of porous media is the intrinsic property of porous media, independent of the fluid. When the compressibility of the fluid is considered, Eq. 1 is modified as follows

$$\frac{P_i^2 - P_o^2}{2PL} = \frac{\eta}{K_1} V_s, \tag{2}$$

where P is the fluid pressure at which V_s is measured.

Darcy's law considers only the viscous effects on the fluid pressure drop at very low flowing velocity. However, fluid flow through porous media usually deviates from Darcy's law with the increase of fluid velocity due to the contribution of inertia and turbulence. Forchheimer's equation, yielding more realistic and reliable permeability constants, has been proposed for the incompressible fluid as [21–23]

$$\frac{P_i - P_o}{L} = \frac{\eta}{K_1} V_s + \frac{\rho}{K_2} V_s^2, \tag{3}$$

where K_2 is the non-Darcian or inertial permeability (m). The first term ($\eta V_s/K_1$) represents viscous energy losses and prevails at low fluid velocity, while the second term ($\rho V_s^2/K_2$) represents inertia energy losses and is more significant at high fluid velocity. When the compressibility of the fluid is considered, Eq. 3 is modified as follows

$$\frac{P_i^2 - P_o^2}{2PL} = \frac{\eta}{K_1} V_s + \frac{\rho}{K_2} V_s^2. \tag{4}$$

Considering the contribution of the inertia energy losses and gas compressibility as well as the viscous energy losses, Forchheimer's equation for the compressible gas is best model to evaluate the permeability of porous media [20, 23]. Therefore, Eq. 4 was adopted to calculate the permeability of porous SiC ceramics in this work.

Experimental

Mullite-bonded porous SiC ceramics were fabricated by an in-situ reaction bonding process, described elsewhere [6, 24]. Briefly, the powder mixture of α-SiC, Al_2O_3 and graphite powder was compacted and subsequently sintered at 1,350–1,500 °C for 4 h in air. Graphite is burned out to produce pores and the surface of SiC is oxidized to SiO_2 at high temperature. With further increasing the temperature, the amorphous SiO_2 converts into cristobalite and reacts with α-Al_2O_3 to form mullite. SiC particles are bonded by mullite and the oxidation-derived SiO_2 to obtain porous SiC ceramics. Table 1 show the characterization of the samples adopted in this work.

Table 1 Characterization of the samples adopted in this work

Sample	SiC:Al_2O_3 in green bodies (by volume)	Graphite content in green bodies (vol.%)	Sintering temperature (°C)
S1	3.65	0	1,450
S2	3.65	14.0	1,450
S3	3.65	27.2	1,450
S4	3.65	39.3	1,450
S5	3.65	39.3	1,350
S6	3.65	39.3	1,400
S7	3.65	39.3	1,500

The specimens were machined as the disks of 20.0 mm in diameter and 3.0 mm in thickness for the permeability measurement. Experimental evaluation of N_2 permeability was conducted at room temperature (25 °C; for N_2, $\eta = 1.78 \times 10^{-5}$ Pa·s and $\rho = 1.16$ kg/m^3) by a homemade permeability apparatus. Figure 1 shows the schematic diagram of the permeability apparatus. Nitrogen gas was supplied by the N_2 supply (1) and the output pressure was adjusted by pressure valve (2). The tested samples were fixed in the sample holder (4) between two chambers, leaving a circular gas-passing area. Subsequently, an inlet N_2 pressure (P_i) was applied to the samples and the volumetric N_2-flow rate (Q) was measured under steady-state conditions at ambient pressure (0.1 MPa) by gas flow meter (5). The inlet pressure and the outlet pressure (P_o) were measured by gas manometer (3). The volumetric N_2-flow rate (Q) was converted to N_2 velocity (V_s) using the expression $V_s = 4Q/\pi D^2$, where $D = 15.0$ mm is the sample diameter. Experimental data were fitted to Eq. 4 to obtain the permeability constant K_1 and K_2.

Microstructure of mullite-bonded porous SiC ceramics was observed by scanning electron microscopy (SEM) (Model JSM-5600LV, JEOL, Japan). Pore size distribution was characterized by the mercury porosimetry (Model PoreSizer 9320, Micromeritics, USA). Open porosity was determined by the Archimedes method, where the distilled water was used as the liquid medium.

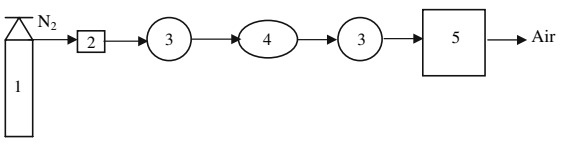

1-N_2 supply, 2-Pressure valve, 3-Gas manometer, 4-Sample holder, 5-Gas flow meter

Fig. 1 Schematic diagram of permeability apparatus developed in this work

Results and discussion

Figure 2 shows the typical microstructure of as-fabricated porous SiC ceramics (sample S2). The stable structure with obviously connected pores was observed. A large number of pores exist among SiC particles and the pore size ranges from submicron to 20 μm. Figure 3 shows the further pore size distribution of the sample (sample S2). It takes on a narrow and bimodal pore size distribution at 1.6 and 8.0 μm, indicating that the texture of porous SiC ceramics is dominated by these two kinds of pores.

Figure 4 shows the open porosity and permeability of samples sintered at different temperatures for 4 h. For all the samples adopted, Darcian permeability K_1 is in the same order of magnitude of 10^{-13} m^2 while non-Darcian permeability K_2 is in the order of magnitude of 10^{-6} m. The

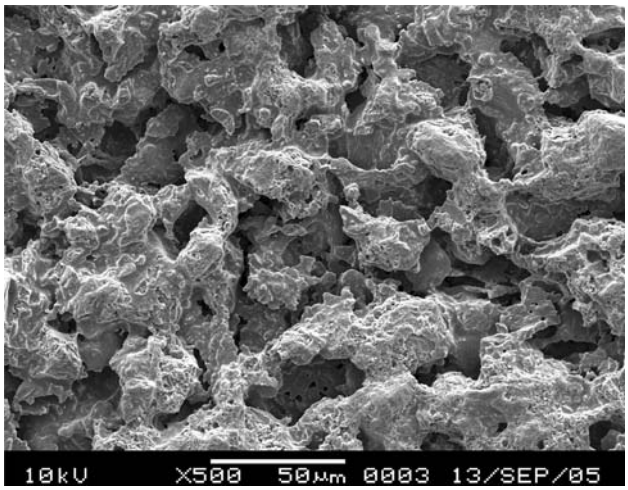

Fig. 2 SEM micrograph of mullite-bonded porous SiC ceramics (sample S2)

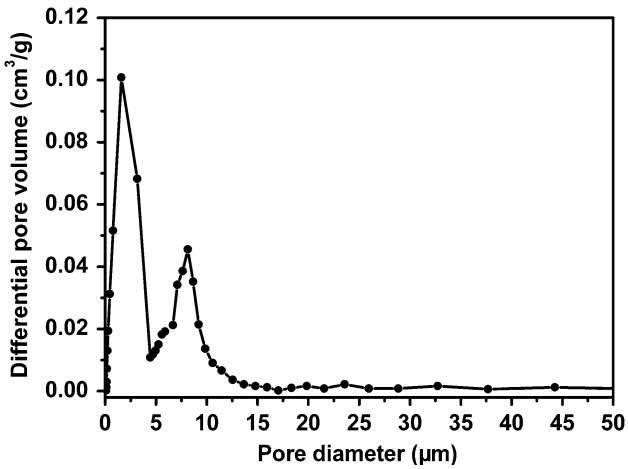

Fig. 3 Pore size distribution of mullite-bonded porous SiC ceramics (sample S2)

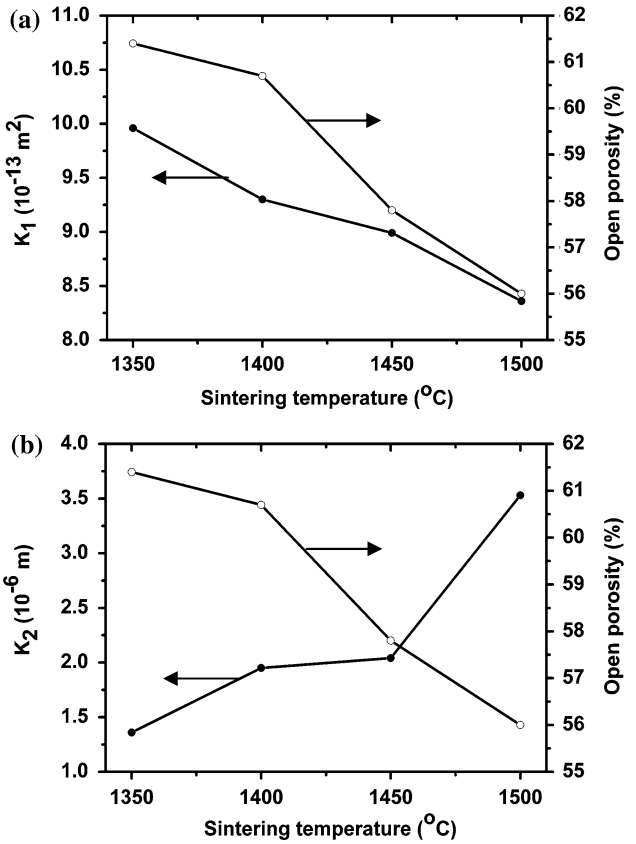

Fig. 4 Open porosity, (**a**) Darcian permeability K_1 and (**b**) non-Darcian permeability K_2 of samples sintered at different temperatures

increased sintering temperatures lead to a gradual decrease in open porosity and Darcian permeability, but a slight increase in non-Darcian permeability. Higher sintering temperatures result in more oxidation-derived SiO_2 with low viscosity which accelerates the formation of mullite by viscous flowing. Acute viscous flow promotes the closure of small pores and the shrinkage of large pores, leading to the decrease in open porosity and pore size. At the same time, viscous flowing effect of SiO_2 impairs the connectivity of open pores and then enlarges the tortuosity of pore channels.

According to Carman–Kozeny's relation [18]:

$$K_1 = \frac{pd^2}{16 f_{CK} \tau^2}, \tag{5}$$

where K_1 is Darcian permeability; p is the efficient porosity contributing to the permeability; d is the average pore diameter; f_{CK} is Carman–Kozeny coefficient; and τ is the tortuosity of pore channels defined by the ratio between the mean length actually traveled by the fluid passing through the porous medium and the thickness of the porous medium in the macroscopic direction of the flow, Darcian permeability is in direct proportion to the efficient porosity and the

square of the average pore diameter but in inverse proportion to the square of the tortuosity. Efficient porosity is mainly contributed by the interconnected open pores going from one side to another of the porous sample. For high porous materials, the efficient porosity approaches the open porosity. Therefore, the decrease in the open porosity and pore diameter and the increase in the tortuosity reduce the Darcian permeability as sintering temperatures rise. With increasing the sintering temperatures, the dead-end porosity increases and more tortuous flow paths are generated. Then, the inertia interaction between gas and porous walls is enhanced even though the open porosity and pore diameter decrease slightly, resulting in the increase of inertia energy losses of flowing gas. Thus, the non-Darcian or inertial permeability increases with the sintering temperatures.

Figure 5 shows the open porosity and permeability of samples with different graphite additions in green bodies. The open porosity, Darcian permeability K_1 and non-Darcian permeability K_2 of porous SiC ceramics increase to a great extent as the graphite content in green bodies increases. Porous SiC ceramics with 14.0 vol.% graphite addition possess 1.7 times open porosity, 23.8 times K_1 and 1857.1 times K_2 of porous SiC ceramics without graphite content.

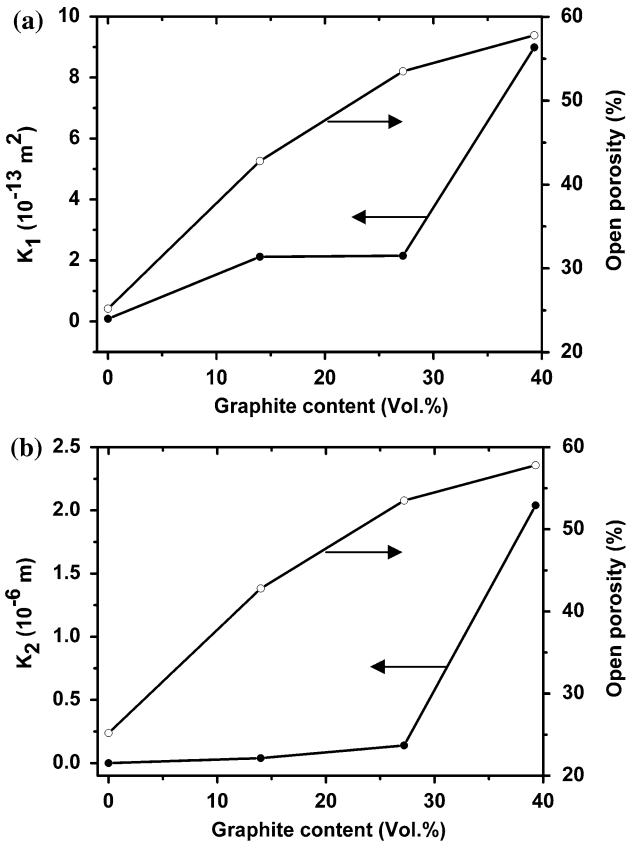

Fig. 5 Open porosity, (**a**) Darcian permeability K_1 and (**b**) non-Darcian permeability K_2 as a function of graphite additions

In porous SiC ceramics, there are mainly two kinds of pores which correspond to two peaks in the curve of pore size distribution, as shown in Fig. 3. Small pores with ~1.6 μm derive from the stack of SiC particles while large pores with ~8.3 μm are formed by burning out graphite particles [24]. More graphite additions in green bodies increase the number of the large pores, resulting in the higher open porosity. The high porosity improves the connectivity of open pores and then reduces the tortuosity of pore channels. Furthermore, plenty of large pores by burning out graphite particles enlarge the average pore diameter in porous SiC ceramics. According to Eq. 5, the higher open porosity, larger average pore diameter and lower tortuosity lead to the larger Darcian permeability. Therefore, Darcian permeability of porous SiC ceramics increases with the graphite content. Due to the abrupt increase of the open porosity and pore size caused by the addition of graphite, more pore walls were formed. Then, the interaction between the flowing gas and pore walls is enhanced. The texture—non-Darcian permeability K_2 relation of porous ceramics can be well-described by the following equation [21]

$$K_2 = \frac{ap^3 d}{1-p}, \tag{6}$$

where a is the empirical constant depending on the pore shape and the tortuosity. Consequently, the addition of graphite improves the non-Darcian permeability by enlarging the open porosity and pore size.

Conclusions

The N_2 permeability behavior of mullite-bonded porous SiC ceramics with the open porosity of 25–62% and the bimodal pore size distribution between submicron and 20 μm was investigated at room temperature. The results show that Darcian permeability is in the order of magnitude of 10^{-13} m^2 while non-Darcian permeability K_2 is in the order of magnitude of 10^{-6} m. With the increase of sintering temperatures, Darcian permeability of samples decreases because of the lower open porosity and smaller pore size. In addition, higher sintering temperatures generate more tortuous flow paths in porous ceramics which enhance the inertia interaction between the flowing gas and the pore walls, resulting in the higher non-Darcian permeability. However, the addition of graphite improves the Darcian and non-Darcian permeability by enlarging the open porosity and pore size.

Acknowledgements The authors thank for the financial support from the ''Plan of Outstanding Talents'' of Chinese Academy of Sciences. The comments of the reviewers are greatly appreciated.

References

1. Greil P (2002) Adv Mater 14:709
2. She JH, Deng ZY, Daniel-Doni J, Ohji T (2002) J Mater Sci 37:3615
3. Montanaro L, Jorand Y, Fantozzi G, Negro A (1998) J Eur Ceram Soc 18:1339
4. Zhu X, Jiang D, Tan S (2002) Mater Sci Eng A323:232
5. Ihle J, Herrmann M, Adle J (2005) J Eur Ceram Soc 25:987
6. Ding S, Zhu S, Zeng Y, Jiang D (2006) Ceram Int 32:461
7. Zhu X, Jiang D, Tan S (2001) Mater Res Bull 36:2003
8. Sepulveda P, Binner JP (1999) J Ceram Soc Jpn 19:2059
9. Zhu S, Ding S, Xi H, Wang R (2005) Mater Lett 59:595
10. She JH, Ohji T, Deng ZY (2002) J Am Ceram Soc 85:2125
11. Ding S, Zeng Y, Jiang D (2006) J Inorg Mater 21:1397
12. Latella BA, Henkel L, Mehrtens EG (2006) J Mater Sci 41:423
13. de Souza Rodrigues C, Ghavami K, Stroeven P (2006) J Mater Sci 41:6925
14. Glass SJ, Green DJ (1999) J Am Ceram Soc 82:2745
15. Innocentini M, Pandolfelli V (2001) J Am Ceram Soc 84:941
16. Lukasiewicz SJ, Reed JS (1998) J Am Ceram Soc 71:1008
17. Ohzawa Y, Nomura K, Sugiyama K (1998) Mater Sci Eng A255:33
18. Carman PC (1956) Flow of gases through porous media. Butterworths, London
19. Collins RE (1961) Flow of fluids through porous materials. Reinhold, New York
20. Innocentini M, Pardo A, Salvini V, Pandolfelli V (1999) Am Ceram Soc Bull 78:64
21. Ergun S (1952) Chem Eng Prog 48:89
22. Philipse AP, Schram HL (1991) J Am Ceram Soc 74:728
23. Innocentini M, Pardo A, Salvini V, Pandolfelli V (2000) J Am Ceram Soc 83:1536
24. Ding S, Zhu S, Zeng Y, Jiang D (2007) J Eur Ceram Soc 27:2095